Journal of Aerosol Science 169 (2023) 106140

Contents lists available at ScienceDirect

Journal of Aerosol Science

journal homepage: www.elsevier.com/locate/jaerosci

Correction for particle loss in a regulatory aviation nvPM emissions system using measured particle size

Eliot Durand [a,*], Lukas Durdina [b], Greg Smallwood [c], Mark Johnson [d], Curdin Spirig [b], Jacinta Edebeli [b], Manuel Roth [b], Benjamin Brem [e], Yura Sevcenco [a], Andrew Crayford [a]

[a] Cardiff School of Engineering, Cardiff University, Wales, CF24 3AA, UK
[b] Centre for Aviation, ZHAW Zurich University of Applied Sciences, CH, 8401, Winterthur, Switzerland
[c] Metrology Research Centre, National Research Council Canada, Ottawa, Ontario, K1A 0R6, Canada
[d] Rolls-Royce, plc, Sin A-37 PO Box 31, Derby, DE24 8BJ, UK
[e] Laboratory of Atmospheric Chemistry, Paul Scherrer Institute, CH, 5232, Villigen PSI, Switzerland

ARTICLE INFO

Keywords:
Particle transport loss
Aviation nvPM
Particle size distribution
Sampling system loss correction

ABSTRACT

To reduce the adverse impact of civil aviation on local air quality and human health, a new international standard for non-volatile Particulate Matter (nvPM) number and mass emissions was recently adopted. A system loss correction method, which accounts for the significant size-dependent particle loss, is also detailed to predict nvPM emissions representative of those at engine exit for emissions inventory purposes. As Particle-Size-Distribution (PSD) measurement is currently not prescribed, the existing loss correction method uses the nvPM number and mass measurements along with several assumptions to predict a PSD, resulting in significant uncertainty.

Three new system loss correction methodologies using measured PSD were developed and compared with the existing regulatory method using certification-like nvPM data reported by the Swiss and European nvPM reference systems for thirty-two civil turbofan engines representative of the current fleet. Additionally, the PSD statistics of three sizing instruments typically used in these systems (SMPS, DMS500 and EEPS) were compared on a generic aero-engine combustor rig.

General agreement between the three new PSD loss correction methods was observed, with both nvPM number- and mass-based system loss correction factors (k_{SL_num} and k_{SL_mass}) within ±10% reported across the engines tested. By comparison, the existing regulatory method was seen to underpredict k_{SL_num} by up to 67% and overpredict k_{SL_mass} by up to 49% when compared with the measured-PSD-based methods, typically driven by low nvPM mass concentrations and small particle size. In terms of the particle sizing instrument inter-comparison, an agreement of ±2 nm for the GMD and ±0.08 for the GSD was observed across a range of particle sizes on the combustor rig. However, it was seen that these differences can result in a 19% bias for k_{SL_num} and 8% for k_{SL_mass} for the measured-PSD-based methods, highlighting the need for further work towards the standardisation of PSD measurement for regulatory purposes.

* Corresponding author. Cardiff University, School of Engineering, Queen's Buildings, 14-17 The Parade, Cardiff, CF24 3AA, UK.
E-mail address: DurandEF@cardiff.ac.uk (E. Durand).

https://doi.org/10.1016/j.jaerosci.2023.106140
Received 18 November 2022; Received in revised form 13 January 2023; Accepted 19 January 2023
Available online 24 January 2023

1. Introduction

Abbreviations

Symbol	*Definition*
AFR	Air to Fuel Ratio
AIR	Aerospace Information Report
APC	Aerosol Particle Counter
ARP	Aerospace Recommended Practice
CH	Swiss
CPC	Condensation Particle Counter
DF_1	Dilution factor in the main diluter of a nvPM regulatory system
DF_2	Second stage (VPR) dilution factor in the nvPM number instrument
DMA	Differential Mobility Analyser
DMS500	Differential Mobility Spectrometer
EEP	Engine Exit Plane
EEPS	Engine Exhaust Particle Sizer
EUR	European
GMD	Geometric Mean Diameter
GSD	Geometric Standard Deviation
ICAO	International Civil Aerospace Organization
k_{SL_num}	nvPM number system loss correction factor
k_{SL_mass}	nvPM mass system loss correction factor
LOQ	Limit Of Quantification
nvPM	Non-volatile Particulate Matter
MSD	Mass-space Particle Size Distribution
N/M	Number to Mass ratio (nvPM)
PM	Particulate Matter
PSD	Particle Size Distribution (Number-space)
PSD_B	Particle Size Distribution Bin-by-bin
PSD_{L1}	Particle Size Distribution 1 Lognormal fit
PSD_{L2}	Particle Size Distribution 2 Lognormal fits
RQL	Rich-burn, Quick-mix, Lean-burn
RAPTOR	Research of Aviation PM Technologies, mOdelling and Regulation
$R_{N/M}$	Regulatory Number to Mass ratio
Slpm	Standard litre per minute
SMPS	Scanning Mobility Particle Sizer
STP	Standard Temperature and Pressure
VPR	Volatile Particle Remover

Combustion-generated pollutants have been increasingly studied and regulated owing to their adverse health and climate impacts, with the aviation sector globally contributing to ~3.5% of effective radiative forcing (Lee et al., 2021). While the effect of combustion-generated gases on health and the environment is well established, the impact of particulate matter (PM) is less known (Bendtsen et al., 2021). Adverse health effect of particles is strongly linked to their size, with the relatively small PM emitted by aviation gas turbine engines (mean electrical mobility diameter typically between 15 and 40 nm (Boies et al., 2015; Delhaye et al., 2017; Durand et al., 2021; Durdina et al., 2019)) capable of penetrating deep into the lungs and reaching the systemic circulation (Bendtsen et al., 2021; Jonsdottir et al., 2019).

In response to the aforementioned concerns, a non-volatile PM (nvPM) certification requirement and emissions standard was adopted by the International Civil Aviation Organization (ICAO) for civil aviation turbofan and turbojet engines with rated thrust >26.7 kN (ICAO, 2017), replacing the legacy smoke number standard. In the standard, nvPM are defined as particles present at the aircraft engine exit plane which do not volatilise when heated to 350 °C. To afford traceable and repeatable measurement of nvPM in various sized engine testing facilities, a long (~30–35m) standardised sampling and measurement system is prescribed, which samples exhaust directly at the aircraft Engine Exit Plane (EEP) before diluting, cooling and conditioning (SAE International, 2020, 2021). This, combined with the small size of nvPM emitted from commercial aircraft engines, results in significant particle loss prior to measurement, up to 50% for nvPM mass and 90% for nvPM number (SAE International, 2019).

Accurate particle loss correction is therefore critical for predicting nvPM emissions at the source (i.e., EEP) relevant for modelling and air quality emission inventories, and improving combustion technologies, even if currently not required for engine nvPM emissions certification. Hence, a system particle loss correction methodology was recently added to the ICAO Annex 16 vol II (ICAO, 2017).

However, particle loss is known to be size-dependent, and particle size measurement is not currently prescribed. Therefore, the current system loss correction methodology requires the use of the reported nvPM number and mass, along with several limiting assumptions, to derive a particle size distribution (PSD) and associated losses, which results in uncertainty in the reported EEP nvPM emissions available in the ICAO Engine Emissions Databank (EEDB, 2021). Limited studies report EEP nvPM concentrations (i.e., fully corrected for system loss) and these employ different correction methodologies (Corbin et al., 2022; Durdina et al., 2021; Harper et al., 2022; Saffaripour et al., 2019).

Particle size measurement is currently not prescribed in the aerospace regulatory standard due to issues associated with the definition of and traceable measurement of nvPM size. The impact of the representativeness of the fractal nvPM witnessed in gas turbine exhaust, along with a lack of standard measurement and calibration practices for size instruments, therefore need further investigation. However, fast-sizing instrument capabilities have significantly improved in the last decades, with PSD becoming critical engineering information for combustor design and environmental impact assessment. PSD measurement can also facilitate system loss correction, reducing uncertainties compared to the existing system loss method which requires several assumptions (e.g., particle density, lognormality, GSD) and uses nvPM mass and number measurements as input. Recently, three commercially available size spectrometers have been demonstrated on ICAO compliant nvPM systems (Durand et al., 2021; Kinsey et al., 2021; Xue et al., 2015), namely: the scanning mobility particle sizer (SMPS, TSI Inc.), the differential mobility spectrometer (DMS500, Cambustion Ltd) and the engine exhaust particle sizer (EEPS, TSI inc.), all reporting size as electrical mobility diameters, which is typically used for theoretical particle penetration efficiency calculation (Baron et al., 2011; Durand et al., 2020). Other real-time particle size measurement instruments measuring in aerodynamic space are available (ELPI, Dekati Ltd.; APS, TSI Inc.; AMS, Aerodyne Research Inc.), with the aerodynamic diameter being a more relevant parameter for assessing the impact of PM on health (D. Kittelson, Khalek, et al., 2022). Few studies have compared the sizing performance of particle size instruments for combustion aerosol (Xue et al., 2015; Zimmerman et al., 2014).

In this study, the uncertainty associated with particle size measurement of two Cambustion DMS500, a TSI EEPS, and a TSI SMPS was assessed using aviation-like nvPM from a Rich-burn, Quick-mix, Lean-burn (RQL) generic combustor rig. Measured PSD was then used to develop three system loss correction methodologies deemed suitable for nvPM regulatory systems. The three measured-PSD-based system loss correction methodologies were subsequently assessed and compared with the currently prescribed system loss method using certification-like nvPM emissions data collected by the European (EUR) and Swiss (CH) nvPM reference systems covering thirty-two gas turbine engines from seven engine manufacturers, with rated thrusts from $<$26.7 kN (business aviation) to $>$300 kN (long haul) hence representative of the current commercial fleet. Finally, the impact of PSD measurement uncertainty on the measured-PSD-based system loss correction methodologies was evaluated.

2. Material and methods

2.1. Experimental nvPM data collection

This study compiles novel experimental nvPM datasets, collected over five years of emissions testing by the European (EUR) and Swiss (CH) nvPM reference systems, which were operated in compliance with both the ICAO standard (ICAO, 2017) and SAE ARP 6320 (SAE International, 2021) during full-scale engine and combustor rig testing. Further details of the two compliant systems are detailed in the literature (Crayford et al., 2014; Lobo et al., 2015, 2020).

To enable this study, additional PSD measurements were undertaken during all testing opportunities providing PSD statistics required for system loss correction, namely the statistical Geometric Mean Diameter (GMD), Geometric Standard Deviation (GSD) and PSD shape. During all certification-like engine testing data reported in this study, a Cambustion Differential Mobility Spectrometer (DMS500) measuring from 5 to 1000 nm was employed with the EU nvPM reference system and a TSI Scanning Mobility Particle Sizer (SMPS) composed of a long Differential Mobility Analyser (DMA) model 3081A, a bipolar Kr-85 charger model 3077A and a TSI 3776 Condensation Particle Counter (CPC) configured to measure typically from 7.9 to 242 nm was employed with the CH nvPM reference systems.

To first provide confidence in comparing PSDs reported from the two reference systems, a wider particle size instrument inter-comparison was undertaken as part of the EU CleanSky2 RAPTOR programme. Four particle size instruments were employed, namely: two DMS500s (one from the EU nvPM reference system and one from the National Research Council Canada, respectively labelled DMS 1 and DMS 2 from here on), a loaned TSI EEPS (model 3090) measuring from 5.6 to 560 nm, and the TSI SMPS (model 3938) from the CH nvPM reference system.

The three instrument technologies are based on the same principle of particle charge to drag ratio with all instruments reporting particle size distributions in equivalent electrical mobility space. The DMS500 and EEPS are fast scanning analysers (up to 10 Hz), allowing for transient measurements. They require a mathematical model (i.e., a calibration matrix) to correct for their unipolar charging efficiency and to convert the measured electric current from charged particles hitting their electrometers into a PSD. The SMPS also requires a complex data inversion to determine the PSD, but unlike the fast analysers, it employs bipolar charging and the PSD is based on the CPC-counted monodisperse aerosol downstream of the DMA ("ISO 15900:2009" 2014). The SMPS scans were typically 30–45 s, including retrace and purge time.

The two DMS500s were processed using the monomodal aggregate inversion matrix generated with mini-CAST soot, while the EEPS was processed using the compact inversion matrix generated using spherical particles, as there is no soot calibration matrix representative of gas turbine soot provided by TSI for this instrument. A diesel soot inversion matrix was available for the EEPS, but it was deemed less representative of aviation nvPM than spherical particles given diesel soot is relatively larger and more aggregated

than aviation PM (Baron et al., 2011; Dastanpour & Rogak, 2014). The SMPS was processed using the multiple charge and diffusion corrections. Additionally, to allow a direct comparison of the total number concentration, the SMPS and the EEPS were corrected to Standard Temperature and Pressure (STP). It is noted that some of the particle size data (DMS 1 and EEPS) used in this research was taken outside of the 12-month service and calibration period recommended by the respective instrument manufacturers.

A schematic representation of the particle size intercomparison experiment is depicted in Fig. 1. The DMS500s, EEPS and SMPS sampled exhaust from Cardiff University's Gas Turbine Research Centre's high pressure RQL combustor rig, described in detail elsewhere (Harper et al., 2022), operating at different air-to-fuel-ratios (AFR) with two fuels, namely: a high sooting conventional Jet-A and a low sooting Fischer Tropsch (FT) Gas-To-Liquid (GTL) JET-A (75:25) blend. The exhaust sample was first diluted by a PALAS VKL-10ED to provide the required flow, suppress condensation, and ensure good mixing before being split using a flow splitter (Grimm model 5483) used without the critical orifice to minimise the pressure drop. The flow splitter was connected to the size instruments using 3/8″ inner diameter electrically conductive silicone tubing made as short as practicable (<1 m), with particle losses to the different instruments virtually identical. A total of six 1-min-long test points (each equivalent to two SMPS scans) at a stable condition were performed, with measured GMD between 24 and 42 nm and including one repeat point at a given condition to showcase rig stability and repeatability, as discussed in section 3.1.

Following the assessment of the relative agreement of the size instruments, previously collected data by the EUR and CH regulatory sampling and measurement systems were re-assessed to specifically look at the applicability of measured-PSD-based system loss correction compared to the currently defined methodology. A schematic representation highlighting the general layout of the compliant sampling systems when deployed independently at certification-like engine tests is shown in Fig. 2a. As shown, additional PSD measurement was made on an ancillary sampling port near the nvPM number Aerosol Particle Counter (AVL APC) and mass (AVL MSS or Artium Technologies LII300) instruments.

Finally, to assess the uncertainty associated with PSD instrument model and sampling location, data obtained during parallel testing of the EUR and CH nvPM reference systems was assessed, with details of the experimental setup and locations of PSD instruments highlighted in Fig. 2b. Again, the high pressure RQL combustor rig was utilised, operating at different AFRs on numerous aviation fuels to offer a wide range of particle GMDs and concentrations, as discussed in detail elsewhere (Harper et al., 2022). As can be seen, the DMS 2 was located either near the inlet-probe (position L1), sampling undiluted exhaust, or at the vent of the diluter (position L2) on the EUR nvPM reference system, while the SMPS was either sampling from the diluter vent (position L2) or near the nvPM instruments (position L3) on the CH nvPM reference system. This setup afforded real-time measurement of particle loss in the full sampling system by comparing the PSDs of DMS 1 and DMS 2 as discussed in the Supplementary Information. It is noted that only the DMS500 was used to sample near the probe inlet, as the SMPS and EEPS could not handle the harsh conditions of the hot undiluted sample. Results detailing the impact of instrument type and location on system loss uncertainty are presented in section 3.3.

2.2. Description of system loss correction methodologies

2.2.1. General description of system loss correction calculation

Four system loss corrections methodologies calculating the nvPM number and mass correction factors (k_{SL_num} and k_{SL_mass}), required to predict EEP-representative concentrations from those measured using a regulatory nvPM sampling system, are discussed in this study. Firstly, the currently prescribed method as defined in ARP 6481 (SAE International, 2019) and labelled in this work as method $R_{N/M}$ as described in section 2.2.3, and three measured-PSD-based methodologies, labelled PSD_{L1}, PSD_{L2} and PSD_B which are further discussed in section 2.2.4.

For all four methods, k_{SL_num} and k_{SL_mass} are calculated in three steps as follows: (a) the penetration efficiency to the nvPM number and mass instruments is calculated using the particle transport model as described in section 2.2.2; (b) a PSD is predicted at the EEP differently depending on the method; (c) k_{SL_num} and k_{SL_mass} are calculated by dividing the EEP PSD to the PSD at the instrument between 10 and 242 nm using equation (1). To calculate k_{SL_mass}, the PSDs are converted into mass-space using equation (2). It is noted that for all particle-size-measurement methods, the particle effective density term cancels itself when calculating k_{SL} and therefore isn't required.

The lower 10 nm size bound was selected for k_{SL_num} in line with the regulatory method measurement given that the number counter must have a minimum 50% counting efficiency at 10 nm and that uncertainty increases significantly for particles <10 nm (SAE International, 2019) as highlighted by the near-zero penetration efficiency <10 nm in Fig. 3. The 242 nm upper size bound was selected to ensure comparability between the different size instruments, given the upper size limit of the SMPS of 242 nm used in this

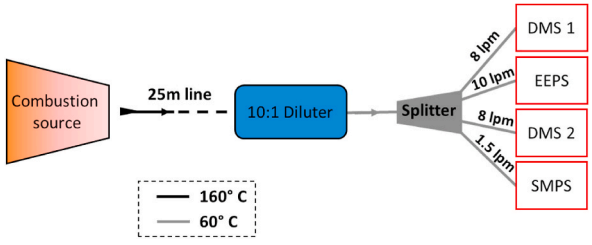

Fig. 1. Diagram of the particle size instrument intercomparison experiment.

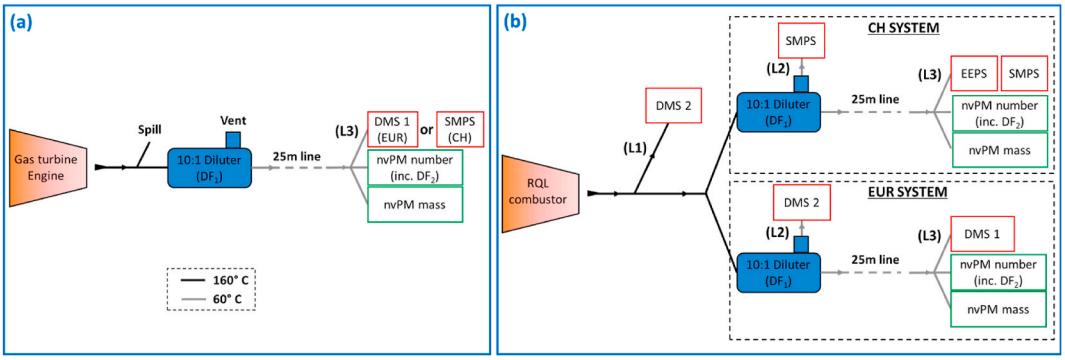

Fig. 2. (a&b): Diagram of the European (EUR) and Swiss (CH) nvPM reference systems used during certification-like gas turbine (a) and RQL combustor rig (b) emission testings including the particle size measurement locations ((L1) near probe-inlet, (L2) diluter vent and (L3) near nvPM instruments).

study.

$$k_{SL\_num/mass} = \frac{\sum_{10\ nm}^{242\ nm} PSD\ at\ EEP_{num/mass\ weighted}(D_p)}{\sum_{10\ nm}^{242\ nm} PSD\ at\ instrument_{num/mass\ weighted}(D_p)} \quad (1)$$

$$Mass(D_p) = Number(D_p) \times Volume(D_p) \times \rho_{eff}(D_p) = Number(D_p) \times \frac{\pi \rho_{eff}(D_p) D_p^3}{6} \quad (2)$$

With D_p the particle size (i.e., size bin from the distribution) and ρ_{eff} the particle effective density (mass/volume of a sphere with same mobility diameter as fractal nvPM particle).

2.2.2. Penetration efficiency calculation

All system loss correction methodologies discussed in this study use the United Technologies Research Center (UTRC) particle transport model, published with the SAE E−31 Aerospace Information Report AIR6241 (SAE International, 2020) and described in the AIR6504 (SAE International, 2022), to calculate the penetration efficiency from the sampling system inlet (i.e., EEP) to a given instrument. The UTRC model predicts particle penetration efficiency by combining gas and particle properties to flow characteristics through user-defined sampling system segments. Particle loss is modelled using equations derived from the literature describing the main deposition mechanisms of ultrafine aircraft nvPM, namely in order of importance diffusional, thermophoretic, inertial, electrostatic and bend loss. Further details of the model and loss mechanisms are discussed in depth elsewhere (Baron et al., 2011; Durand et al., 2020; Hinds, 1998). Experimental validation of the UTRC model on a regulatory-compliant system has been previously demonstrated (D. B. Kittelson, Khalek, et al., 2022; Durand et al., 2020), but only for parts of the system and specific loss mechanisms. Further validation of the UTRC model for a full nvPM regulatory system is provided in the supplementary information. Additional volatile particle remover (VPR) loss corrections are required for the nvPM number instrument penetration due to thermophoresis and diffusion and CPC counting efficiency, as discussed further in ARP6481 (SAE International, 2019).

Typical penetration efficiencies to the nvPM number, mass, and size instruments in a regulatory nvPM sampling system are shown in Fig. 3 for visual aid, with losses <100 nm dominated by diffusion, losses >500 nm caused by the 1 μm cyclone (used to remove large particles shed from the walls). The higher losses witnessed for the nvPM number instrument are due to the additional thermophoretic loss in the prescribed VPR.

Some assumptions were required for the penetration efficiency calculation in this analysis: the penetration efficiency to the number instruments used for k_{SL_num} were calculated using averaged annual calibration data performed by the manufacturer (AVL) post 2018 (three calibrations for the Swiss APC and one calibration for the EUR APC). The AVL calibration certification procedure was updated in 2019, the date from which an additional catalytic stripper after the CAST aerosol source was employed for the VPR penetration efficiency test. It is thought this resulted in higher reported penetration of the smallest particles after this modification, as the semi-volatile soot that would have previously shrunk in the VPR was being removed by the additional catalytic stripper instead. Additionally, since 2019 the calibration of the CPC embedded in the APC has been performed by AVL rather than being performed by TSI, which resulted in slightly different reported counting efficiency at 10 nm due to the different setups and procedures being used by the two calibration laboratories. Additionally, the penetration efficiency in the collection section (i.e., probe inlet to diluter inlet in Fig. 2) used for k_{SL_num} and k_{SL_mass} was calculated for the worst-case scenario corresponding to when the pressure at the inlet of diluter is below ambient and the spill is shut (i.e., flowrate in collection section of ~15 slpm). In practice, the flowrate in the collection section is often higher when sampling high thrust/pressure conditions, however it is noted this has a small impact on the full system penetration efficiency (<2%).

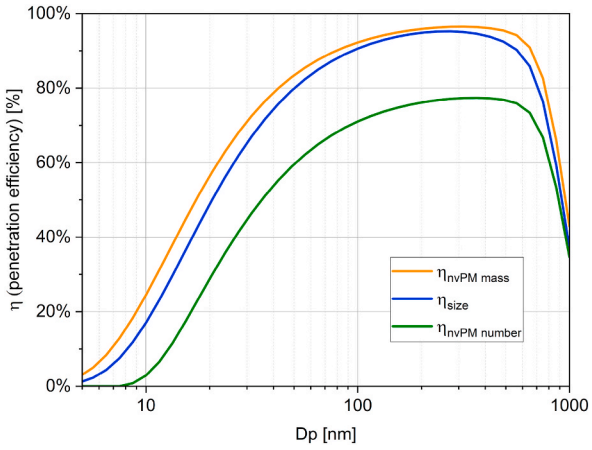

Fig. 3. Example of penetration efficiency to the nvPM number ($\eta_{nvPM\ number}$), mass ($\eta_{nvPM\ mass}$) and size (η_{size}) instruments in a typical regulatory standard sampling and measurement system estimated using the UTRC model.

2.2.3. Description of the regulatory method (method $R_{N/M}$)

The currently prescribed system loss correction method labelled $R_{N/M}$ (regulatory number to mass ratio) uses the measured nvPM number and mass concentration as inputs to predict a PSD at the EEP and system loss correction factors. It generates a PSD at the EEP by minimising the square of the relative difference ($\delta_{method\ R_{N/M}}$) between the measured and calculated particle number to mass concentration (N/M) ratio, as shown in equations (3) and (4) and described in detail in the ARP 6481[1] (SAE International, 2019) and the AIR 6504[1] (SAE International, 2022). It requires several assumptions, the main ones being a particle effective density of 1 g/cm^3, mono-modality and lognormality at the EEP, and a GSD of 1.8.

$$R_{MN}(GMD) = \frac{\sum_{D_p>3nm}^{1000nm} \eta_{mass}(D_p) \times \frac{\pi \rho_{eff} D_p^3}{6} \times e^{-\frac{1}{2}\left\{\frac{\ln(D_p)-\ln(GMD)}{\ln(GSD)}\right\}^2} \times \Delta\ln(D_p)}{\sum_{D_p>3nm}^{1000nm} \eta_{num}(D_p) \times e^{-\frac{1}{2}\left\{\frac{\ln(D_p)-\ln(GMD)}{\ln(GSD)}\right\}^2} \times \Delta\ln(D_p)} \tag{3}$$

$$\delta_{method\ R_{N/M}} = \left\{1 - \frac{R_{MN}(GMD)}{[(k_{thermo} \times DF_1 \times nvPM_{massSTP})/(k_{thermo} \times DF_1 \times DF_2 \times nvPM_{numSTP})]}\right\}^2 \tag{4}$$

Where $\eta_{num/mass}$ is the penetration efficiency to the number/mass instruments, k_{thermo} is the size-independent thermophoretic loss correction factor in the collection section of a regulatory system, DF_1 is the dilution factor in diluter, DF_2 is the second stage (VPR) dilution factor in the number instrument, and $nvPM_{num/mass\ STP}$ is the measured nvPM number and mass at STP conditions (0 °C and 101.325 kPa).

It is noted that while there is no fundamental basis for aerosols to have a lognormal distribution, the various stochastic aspects to condensational growth and coagulation in single-source particle formation processes typically result in a distribution close to lognormal (Seinfeld & Pandis, 2016). Furthermore, the mathematical form of a lognormal distribution is mathematically convenient for describing aerosols (Baron et al., 2011). However, some deviations from lognormality can be observed in traditional RQL aircraft engines (Durand, 2019), where soot is produced and grown in the combustor rich zone, followed by consumption in the mixing and lean zones.

2.2.4. Description of size-measurement-based methods (methods PSD_{L1}, PSD_{L2} and PSD_B)

Three system loss correction methodologies requiring a PSD measurement as an input were developed and are presented, with the Matlab® script detailing these available with the supplementary information. The first method PSD_{L1} (particle size distribution one lognormal) minimises the square of the relative difference between the measured PSD and a mono-modal lognormal PSD at the EEP scaled to the penetration efficiency to the size instrument, as per equation (5). A limitation with methods $R_{N/M}$ and PSD_{L1} is that they only use one lognormal mode at the EEP, making them both unsuitable to deal with bi-modal distributions and monomodal distributions significantly deviating from a lognormal shape. Therefore, a second method PSD_{L2} was designed to operate similarly to method PSD_{L1}; however, it fits the measured PSD with two lognormal distributions at the EEP, allowing it to effectively predict EEP PSDs in the case of bi-modal and non-lognormal monomodal distributions (see illustrative example in Fig. S6 in supplementary information).

[1] An Excel® spreadsheet system loss tool is supplied with ARP 6481 while both the Excel® and a Matlab® system loss tools are provided with AIR 6504.

Finally, a third method PSD_B (particle size distribution bin-by-bin) was developed which doesn't require any fitting. Instead, it directly uses the measured PSD and divides the concentrations in each non-zero size bin by the penetration to the size instrument, as per equation (6). A similar method is used by Cambustion Ltd to correct for particle loss in their catalytic stripper (Cambustion Ltd, 2016, p. Appendix A).

$$\delta_{method\ \mathrm{PSD_{L1}}} = \left\{ 1 - \frac{PSD_{measured}}{\left(\frac{N_{tot}}{\sqrt{2\pi}ln(GSD)} e^{-\frac{1}{2}\left\{ \frac{ln(D_p)-ln(GMD)}{ln(GSD)} \right\}^2} \Delta ln(D_p) \right) \times \eta_{size}(D_p)} \right\}^2 \tag{5}$$

Where N_{tot} (total number concentration), *GMD* and *GSD* are the three variables of a lognormal distribution, and η_{size} is the penetration efficiency to the size instruments.

$$PSD_{EEP_{method\ PSD_B}}(Dp) = \frac{PSD_{measured}(Dp)}{\eta_{size}(D_p)} \tag{6}$$

Finally, once the EEP PSD is generated, the three measured-PSD-based methods calculate k_{SL_num} and k_{SL_mass} similarly to method $R_{N/M}$ by dividing the sum of the EEP PSD by the sum of the PSD at the nvPM number or mass instrument, as per equation (1).

3. Results and discussion

3.1. Particle size instrument intercomparison

The PSDs of the two DMS500s, an EEPS, and a SMPS simultaneously sampling RQL rig combustion exhaust are presented in Fig. 4, with shapes appearing to closely overlap, although the magnitude (i.e., total number concentration) differs slightly. A small inflection can be observed at ~30 nm for the DMS 2 for test points 3 to 5, thought to originate from the calibration uncertainty of the DMS at this size where the singly charged to doubly charged particle split occurs. The corresponding mass-space particle size distributions (i.e., MSD) are also discussed with Fig. S3 in the supplementary information.

Analysis of the PSDs highlighted that the GMD agreed within ±2 nm (i.e., ±5% of the average) and the GSD within ±0.08 (i.e., ±5% of the average) across the size ranges measured, as shown in Fig. 5. DMS 2 typically reported the largest GMD and GSD, while DMS 1 reported the smallest GMD and the EEPS reported the smallest GSD. This witnessed uncertainty in reported PSD is in agreement with literature (Corbin et al., 2022; Xue et al., 2015) and better than the certified accuracy provided by the manufacturers for the fast-scanning instruments (±10% of size standard). This is promising for regulatory use, given that each instrument type was calibrated on a different source using a different protocol as discussed in section 2.1.

It is noted that this analysis is limited to only six test points on RQL combustor exhaust with the GMD ranging from 24 to 42 nm; hence wider disagreement may be observed across larger GMDs and on alternative combustion sources. It is suggested that to get even better closure between the size instruments for aviation gas turbine exhaust measurement, standard measurement and calibration procedures should be adopted as is currently prescribed for aircraft engine nvPM number and mass emission measurements.

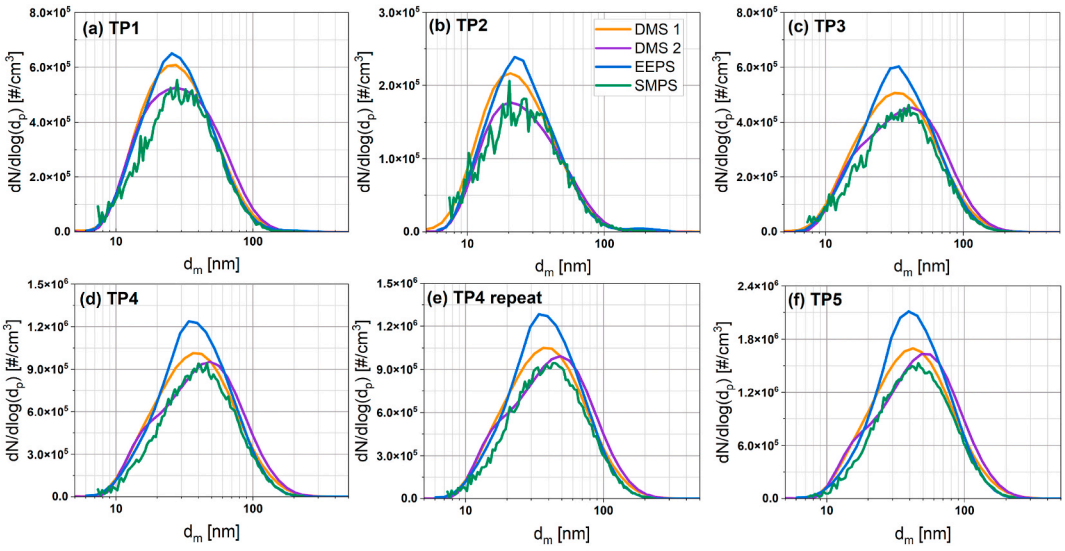

Fig. 4. Measured PSDs (in number counting space) from different instruments for different test points (a–f) during the particle size instrument intercomparison experiment.

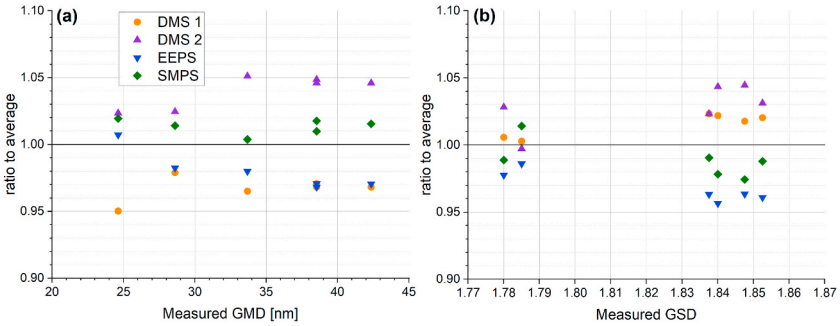

Fig. 5. Ratio of statistical GMD (a) and GSD (b) to the average plotted against measured GMD/GSD for the six test points taken during the particle size instrument intercomparison experiment.

3.2. Aircraft nvPM system loss correction methodologies

3.2.1. Comparison between regulatory and measured-PSD-based system loss correction methods

The nvPM number (k_{SL_num}) and mass (k_{SL_mass}) system loss correction factors for certification-like gas turbine emission testing calculated using method $R_{N/M}$, and methods PSD_{L1}, PSD_{L2}, and PSD_B are presented in Fig. 6. Both k_{SL_num} and k_{SL_mass} increased with decreasing GMD due to the larger diffusional loss at small sizes and ranged between 1.6 – 7.8 and 1.06–2.5, respectively. As can be seen, the three measured-PSD-based methods closely correlated with one another, while method $R_{N/M}$ was more scattered, particularly <25 nm GMD, corresponding to relatively lower measured nvPM mass ~<10 μg/m^3. This increased scatter is thought to originate from the uncertainty associated with nvPM mass measurement approaching an estimated LOQ of 3 μg/m^3 (SAE International, 2019) coupled with shedding events of large particles (>250 nm) re-entrained from the collection cup of the 1-μm cyclone ("RAPTOR Project Library" 2022, p. WP4) prescribed in a regulatory measurement system.

The ratio between method PSD_B and the other system loss correction methods was subsequently calculated. Method PSD_B was chosen as the reference method, given it is the one requiring the least assumption, directly using the measured PSD. The ratio between method $R_{N/M}$ and method PSD_B was on average 0.97 ± 0.16 for k_{SL_num} (ranges between 0.33 and 1.30 in Fig. 7a) and 1.04 ± 0.08 for k_{SL_mass} (ranges between 0.67 and 1.49 in Fig. 8a). While the average agreement between the two methods is good, it can again be seen that method $R_{N/M}$ can significantly underpredict k_{SL_num} and either underpredict or overpredict k_{SL_mass} at measured GMD <25 nm (i.e., measured nvPM mass ~<10 μg/m^3). Generally, the current regulatory prescribed method (method $R_{N/M}$) can be assumed to have an uncertainty of up to 67% for k_{SL_num} and 49% for k_{SL_mass} when compared with method PSD_B. This difference is driven by the assumptions required (section 2.2.3) and the uncertainty associated with the input nvPM number and mass parameters (Lobo et al., 2020).

A better agreement is witnessed between measured-PSD-based methods, with a ratio of method PSD_{L1} to method PSD_B of 1.00 ± 0.03 for k_{SL_num} (scatters between 0.95 and 1.25 in Fig. 7b) and 0.99 ± 0.03 for k_{SL_mass} (scatters between 0.81 and 1.19 in Fig. 8b) although two outliers (outside of the ±20% shaded area) are still present, thought to originate due to significant deviations from lognormality. The best agreement is between method PSD_{L2} and method PSD_B with a ratio of 1.00 ± 0.01 for k_{SL_num} (scatters between 0.94 and 1.09 in Fig. 7c) and 1.00 ± 0.02 for k_{SL_mass} (scatters between 0.90 and 1.10 in Fig. 8c) with no outliers observed from the fit.

It is noted that using a consistent particle size range and resolution (e.g., 10–242 nm) was critical to allow meaningful comparison of the different system loss correction methods, given the particle size instruments measured different size ranges and resolutions affecting method PSD_B, with artifacts appearing <10 nm and >300 nm for some instruments, as discussed in the supplementary

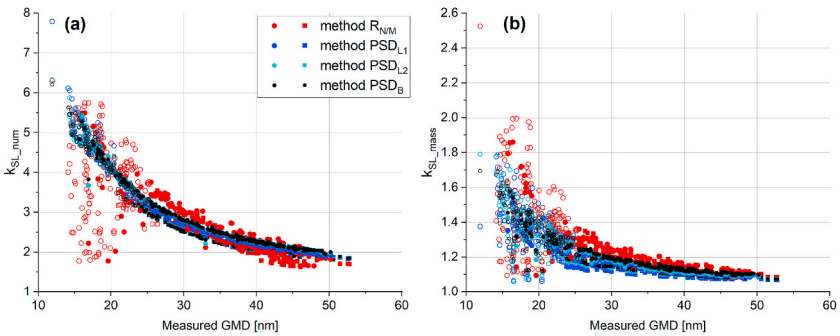

Fig. 6. nvPM number (a) and mass (b) system loss correction factors plotted against measured statistical GMD using different methods (squares represent EUR data, circles represent CH data, filled symbols represent data with measured nvPM mass >10 μg/m^3 and open symbols represent data with measured nvPM mass <10 μg/m^3).

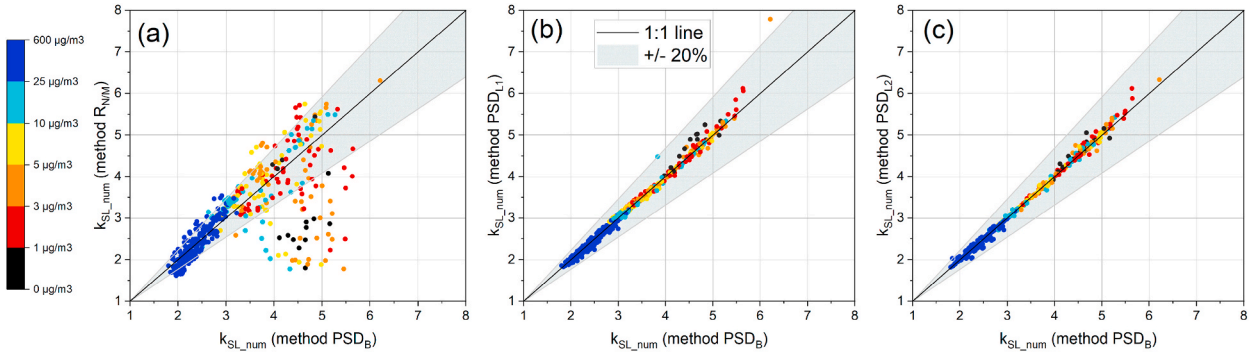

Fig. 7. nvPM number system loss correction factor for method $R_{N/M}$ (a), method PSD_{L1} (b) and method PSD_{L2} plotted against the reference method PSD_B with measured nvPM mass colour mapping. (For interpretation of the references to colour in this figure legend, the reader is referred to the Web version of this article.)

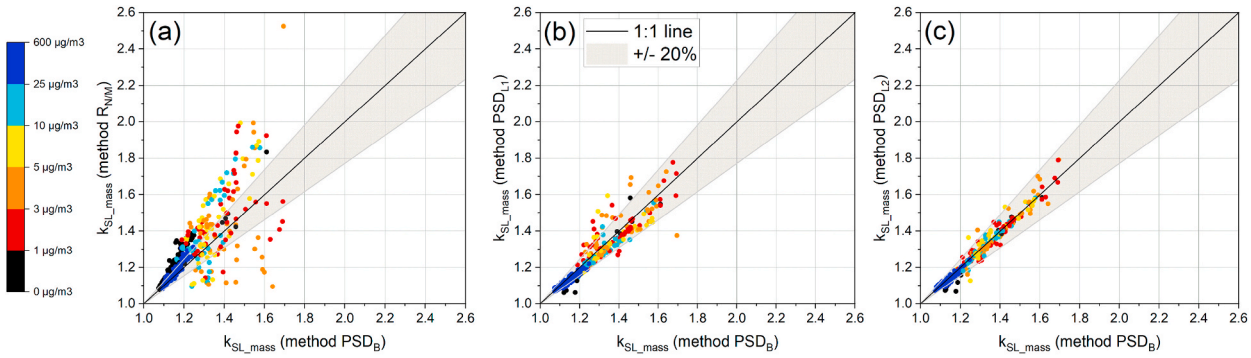

Fig. 8. nvPM mass system loss correction factor for method $R_{N/M}$ (a), method PSD_{L1} (b) and method PSD_{L2} plotted against the reference method PSD_B with measured nvPM mass colour mapping. (For interpretation of the references to colour in this figure legend, the reader is referred to the Web version of this article.)

information.

3.2.2. *Potential improvements of the regulatory method*

Given the limitations associated with the required assumptions, in an attempt to reduce the uncertainty associated with method $R_{N/}$

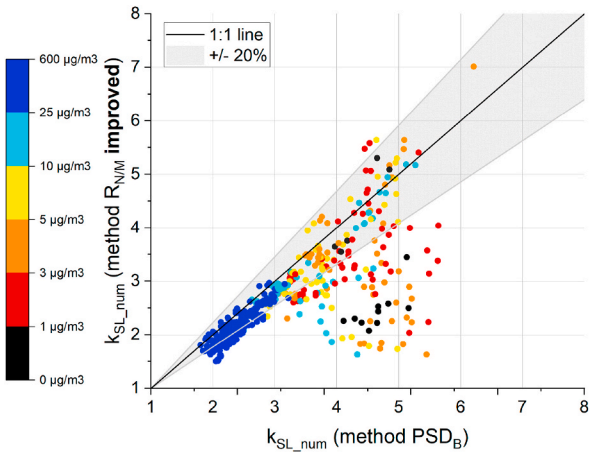

Fig. 9. nvPM number system loss correction factor for method $R_{N/M}$ with improved GSD and particle effective density assumptions plotted against the reference method PSD_B with measured nvPM mass colour mapping. (For interpretation of the references to colour in this figure legend, the reader is referred to the Web version of this article.)

$_{M,}$ k_{sl} outputs were predicted by replacing the fixed GSD (1.8) and density (ρ_{eff} = 1 g/cm^3) assumptions with more representative correlations. The GSD was correlated to the input nvPM N/M using the gas turbine certification-like dataset as shown in Fig. S5 in the supplementary information, and a size-dependent particle effective density derived from the literature ($\rho_{eff} = 0.51 \times (GMD/100)^{-0.52}$) (Olfert & Rogak, 2019). The impact of the improved assumptions was assessed by comparing k_{SL_num} from the improved method $R_{N/M}$ with the reference method PSD_B, as presented in Fig. 9. It was found when comparing Fig. 9 with Fig. 8a that better GSD and particle effective density assumptions did not appear to improve k_{SL_num} correlations between method $R_{N/M}$ "improved" and method PSD_B, with an average ratio of 0.87 ± 0.14 (range from 0.3 to 1.23) observed. This further supports the hypothesis that method $R_{N/M}$ uncertainty is highly influenced by the nvPM number and mass measurement uncertainty ~<10 μg/m^3, and that a single particle effective density assumption is not suitable, given particle density is engine type and power dependent (Durdina et al., 2014).

3.3. Impact of particle size measurement uncertainty on novel system loss corrections

To better understand the potential benefits of the measured-PSD-based system loss correction methods (PSD_{L1}, PSD_{L2} and PSD_B), the uncertainty associated with PSD measurement introduced by different instruments and sampling locations was investigated on k_{SL}. As shown in Fig. 2b, the SMPS, EEPS and DMS500s were positioned at different locations of the EUR and CH regulatory sampling systems during RQL combustor rig testing.

3.3.1. Particle size instrument model uncertainty on measured-PSD-based k_{SL}

The uncertainty arising from the particle size instrument model (DMS 1, DMS 2, SMPS and EEPS) on the k_{SL_num} and k_{SL_mass} derived from method PSD_{L1}, PSD_{L2} and PSD_B was assessed using the size instrument comparison data (section 3.1), with the results shown in Figs. 10 and 11. To ensure comparability, the same system dimensions to the nvPM number and mass instruments were used to calculate k_{SL} with the various PSD input from the different instruments used to predict the EEP PSD as discussed in section 2.2.1. It was seen that the bias introduced by the size instrument model on reported k_{SL} was dependent on the specific method being used, with k_{SL_num} differences constrained within ±4% for method PSD_{L1} (Fig. 10a) and PSD_{L2} (Fig. 10b), and mostly constrained within ±5% for method PSD_B (Fig. 10c). Generally, DMS 1 reported the largest k_{SL_num}, whilst the SMPS reported the smallest. This is thought to stem from the fact that DMS 1 measured the highest concentration of particle <20 nm where losses are the highest, in contrast to the SMPS (see Fig. 4). For k_{SL_mass}, the agreement was generally better, with differences constrained within ±4% for method PSD_{L1} (Fig. 11a), ±3% for PSD_{L2} (Fig. 11b) and ±2% witnessed for method PSD_B (Fig. 11c). It is noted that the quoted differences are defined as the difference between maximum and minimum k_{SL} divided by the average.

3.3.2. Particle size instrument location uncertainty on measured-PSD-based k_{SL}

The impact of the particle size instrument location on system loss correction was assessed by placing the same size measurement instruments at various locations along the respective reference nvPM sampling systems during RQL rig emission testing. Positioning the size instrument nearer to the probe inlet results in lower particle loss to the instrument, meaning more particles are counted by the instrument, and hence less corrections are required to predict an EEP PSD. DMS 2 and SMPS were alternatively located near the probe, at the diluter vent, and near the nvPM number/mass instruments (respectively (L1), (L2) and (L3) in Fig. 2b). Again, to ensure comparability, the same system dimensions to the nvPM number and mass instruments were used to calculate k_{SL} with the various PSD input measured at different locations used to predict the EEP PSD as discussed in section 2.2.1.

The results are presented in Fig. 12 using PSD_B, where both k_{SL_num} and k_{SL_mass} follow the same trend regardless of the size instrument location, with similar results observed with methods PSD_{L1} and PSD_{L2}. This result suggests that the particle size instrument location in a regulatory system does not significantly impact measured-PSD derived k_{SL} uncertainty, further validating the UTRC model as adequate to correct for theoretical sampling loss.

3.3.3. Cumulated particle size measurement uncertainty on measured-PSD-based k_{SL}

The cumulated impact of the particle size instrument model (DMS500, EEPS or SMPS), the particle size measurement location (L1,

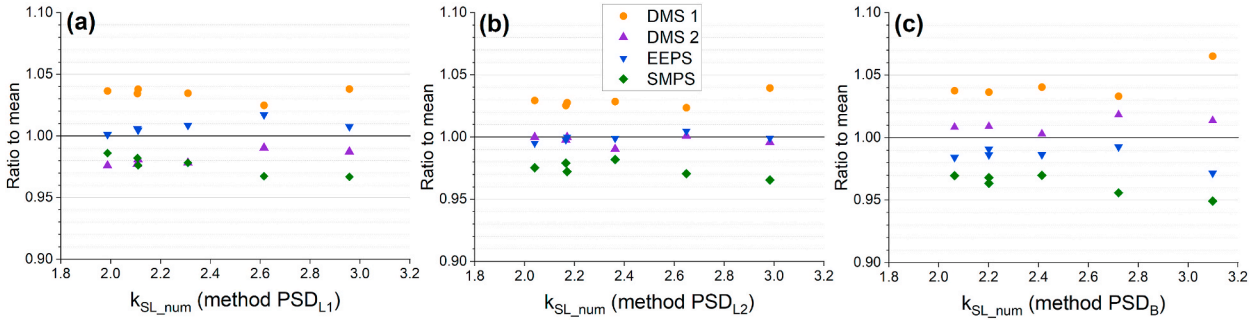

Fig. 10. Ratio of nvPM number system loss correction factor calculated using method PSD_{L1} (a), PSD_{L2} (b) and PSD_B (c) to the average plotted against the correspoding system loss correction factor using PSD data from the particle size instrument intercomparison experiment.

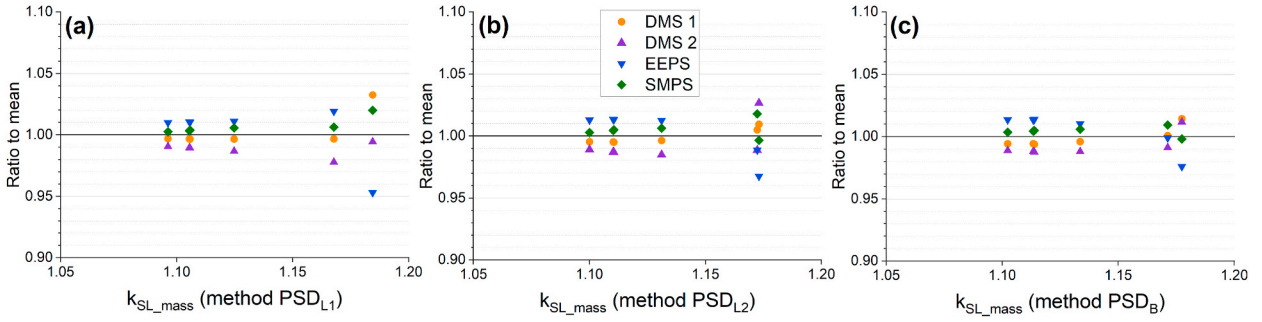

Fig. 11. Ratio of nvPM mass system loss correction factor calculated using method PSD_{L1} (a), PSD_{L2} (b) and PSD_B (c) to the average plotted against the correspoding system loss correction factor using PSD data from the particle size instrument intercomparison experiment.

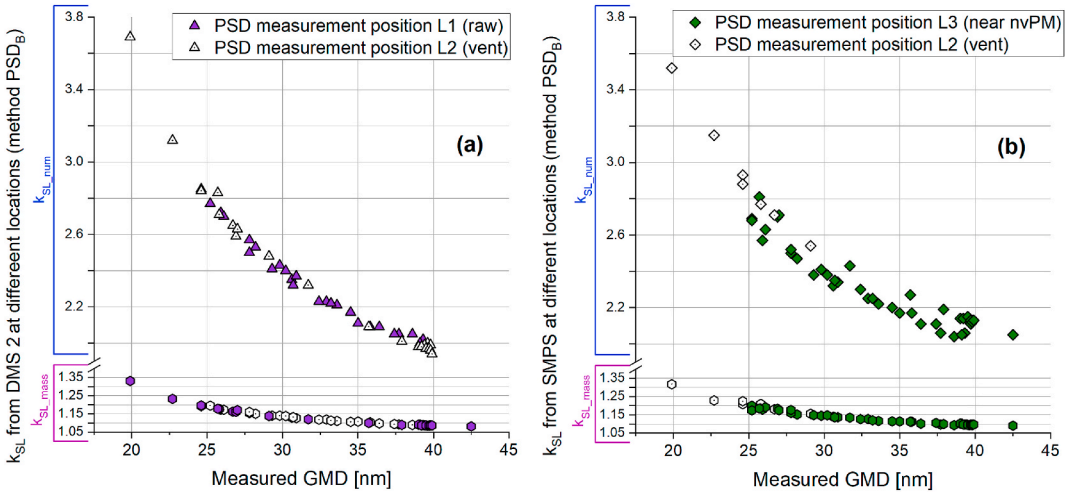

Fig. 12. nvPM number and mass calculated using method PSD_B with (a) DMS 2 at locations L1 and L2, and (b) SMPS at locations L2 and L3 plotted against measured statistical GMD.

L2, L3 in Fig. 2b) and the sampling system used (CH, EUR) was subsequently assessed for PSD_B using a large dataset collected during RQL rig emission testing, with the results presented in Fig. 13. Again, to ensure system loss correction factor comparability, the same system dimensions to the nvPM number and mass instruments were used to calculate k_{SL} with the various PSD input measured using different instruments at different locations used to predict the EEP PSD as discussed in section 2.2.1.

Both k_{SL_num} and k_{SL_mass} were seen to follow the same decreasing trend with increasing GMD regardless of the PSD measurement, brought about as diffusional losses reduce for larger particles. However, a vertical scatter is observed corresponding to the PSD measurement uncertainty on k_{SL}. For a given test point (i.e., GMD), differences of up to 19% were reported for k_{SL_num} (9.5% average difference) and up to 7.7% for k_{SL_mass} (2.4% average difference). The SMPS again generally reported the smallest k_{SL_num} while the EEPS typically reported the largest k_{SL_num} and k_{SL_mass}, suggesting the EEPS measured more of the smaller (<15 nm) and larger (>100 nm) particles when compared with the other size instruments.

In comparison, the difference for the different regulatory systems (CH or EUR) using method $R_{N/M}$ was up to 20.3% for k_{SL_num} (4.2% average difference) and up to 9.1% for k_{SL_mass} (0.6% average difference) for the same dataset. This finding suggests that the impact of current PSD measurement uncertainty on the measured-PSD-based system loss correction methods is marginally smaller than current nvPM number and mass measurement uncertainties.

4. Summary and conclusions

Four methodologies to correct for particle loss in an ICAO regulatory nvPM system were assessed to predict emissions representative of those at engine exit (EEP), namely the current regulatory method ($R_{N/M}$) and three measured-PSD-based methods (PSD_{L1}, PSD_{L2} and PSD_B). Data collected by the EUR and CH nvPM systems, including additional PSD measurement, and covering thirty-two gas turbine engines representative of the current commercial fleet, were used for this analysis.

To first provide confidence in using measured PSD for system loss correction, four particle size measurement instruments (two Cambustion DMS500s, one TSI EEPS and one TSI SMPS) were compared on nvPM from a generic aero engine RQL combustor. The

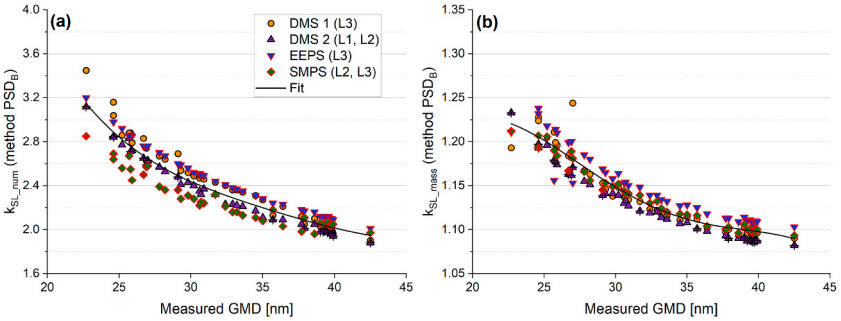

Fig. 13. nvPM number (a) and mass (b) system loss correction factors calculated using method PSD_B with various PSD measurements (different models, locations and sampling systems) during the RQL testing plotted against statistical GMD of the measured PSD (Red edges symbols = EUR system data; Black edges symbols = CH system data; symbols with dots in the centre = PSD measurement position L1/raw; symbols with crosses in the centre = PSD measurement position L2/vent). (For interpretation of the references to colour in this figure legend, the reader is referred to the Web version of this article.)

measured GMD for the different instruments was found to agree within ±2 nm and the GSD within ±0.08 (i.e., ±5%) for particle size distributions typical of aircraft nvPM, demonstrating that these instruments were suitable for measuring aircraft nvPM in a regulatory system.

In the absence of prescribed PSD measurement, method $R_{N/M}$ has been shown to perform relatively well in predicting k_{SL_num} and k_{SL_mass} (i.e., ±20% of measured-PSD-based method) at GMD >25 nm, corresponding to measured nvPM mass >10 μg/m^3. However, k_{SL} uncertainty with method $R_{N/M}$ increased for measured GMD <25 nm when the prescribed nvPM mass measurement approached LOQ, with k_{SL_num} underpredicted by up to 67% and k_{SL_mass} overpredicted by up to 49% when compared with the reference method PSD_B. This is particularly relevant as modern engine technologies and sustainable aviation fuel (SAF) with higher hydrogen content will drive nvPM emissions to be lower in mass and number concentrations and smaller in size, increasing the need for a measured PSD. Also, it was found that method $R_{N/M}$ could not be meaningfully improved with more representative GSD and particle effective density.

The three measured-PSD-based methods agreed to within ±10% for both k_{SL_num} and k_{SL_mass}, with each method having specific advantages and disadvantages. Method PSD_{L1} assumes a single lognormal mode and therefore is not suitable for non-lognormal and multimodal distributions. However, assuming a lognormal distribution minimises the uncertainty associated with the measured PSD shape which can be impacted by the calibration matrix for fast-scanning instruments. Also, given that method PSD_{L1} fits the measured PSD, it can calculate system loss correction factors for any given particle size range and resolution. Method PSD_{L2} has the same advantages as method PSD_{L1} (i.e., user-defined size range and resolution) and can also resolve non-lognormal and multimodal distributions with greater accuracy, and has better closure with method PSD_B, as it can fit two lognormal modes. It is noted that this method could easily be adjusted to include more than two lognormal modes should they be required in the future. Method PSD_B is more straightforward than methods PSD_{L1} and PSD_{L2} as it does not fit the measured PSD and does not assume lognormality. Instead, the measured PSD scaled by the system penetration function is directly used. Both the main advantage and inconvenience of this method is therefore that it solely relies on the measured PSD and that the size range and resolution is fixed by the input PSD. If the PSD measurement is highly accurate and performed at the full relevant size range, then method PSD_B may be considered the best available system loss correction methodology. However, PSD measurement uncertainty can strongly impact its prediction, particularly at the bounds of the measured PSD given the relatively higher losses for the smallest (<20 nm) and largest (>300 nm) particles in a regulatory system.

Overall, method PSD_{L2} is recommended for system loss correction given it can resolve multimodal and non-lognormal distributions (unlike method PSD_{L1}) and can be calculated for any user-input size range and resolution (unlike method PSD_B). It is noted that measured PSDs from the nvPM datasets used in this analysis were generally monomodal and near lognormal. However, the capability of solving more than one mode will be critical with future technologies (e.g., lean burn), sustainable aviation fuels, and towards total PM regulation (volatile and non-volatile modes). It is also noted that it was critical to use a consistent size range (10–242 nm in this analysis) to permit meaningful comparison of the different system loss correction methods, given the size instruments measured PSDs at different size ranges and resolutions, with artifacts sometimes appearing <10 nm and >300 nm when corrected to the EEP.

Finally, to better understand the potential benefits of the measured-PSD-based loss correction methods, the uncertainty associated with PSD measurement introduced by different size instruments and sampling locations within a regulatory nvPM system was investigated. It was found that the particle size instrument model, the measurement location, and the reference sampling system being used were responsible for a bias of up to ~19% for k_{SL_num} and ~8% for k_{SL_mass}. It is recommended that standard calibration and measurement procedures should be adopted for particle size measurement to further reduce the uncertainty associated with system loss correction.

This study demonstrates that adopting measured-PSD-based system loss correction methods would reduce uncertainty for engine-exit-representative nvPM number and mass emissions of aircraft gas turbine engines, resulting in improved modelling and characterisation potential to assess the impact of nvPM emissions on the environment and local air quality. The particle loss correction methodologies discussed in this manuscript can also be applied to any sampling system equipped with PSD measurement.

Declaration of competing interest

The authors declare that they have no known competing financial interests or personal relationships that could have appeared to influence the work reported in this paper.

Data availability

Data will be made available on request.

Acknowledgments

The experimental programme of work received funding from Clean Sky 2 Joint undertaking under the European Union's Horizon 2020 research and innovation RAPTOR programme (Grant agreement ID: 863969).

The authors would also like to acknowledge the Swiss Federal Office of Civil Aviation for funding operation and maintenance of the CH nvPM reference system (projects EMPAIREX SFLV 2015-113, AGEAIR SFLV 2017-030, and AGEAIR 2 SFLV 2018-048), EASA for the loan of the EUR nvPM mobile reference system under contract EASA. 2015.C01.AM01, and Transport Canada for the loan of the Cambustion DMS500 from NRC.

Appendix A. Supplementary data

Supplementary data to this article can be found online at https://doi.org/10.1016/j.jaerosci.2023.106140.

References

Baron, P., Willeke, K., & Kulkarni, P. (2011). *Aerosol measurement, principles, techniques, and applications* (3rd ed.). John Wily & Sons, Inc.

Bendtsen, K. M., Bengtsen, E., Saber, A. T., & Vogel, U. (2021). A review of health effects associated with exposure to jet engine emissions in and around airports. *Environmental Health, 20*(1), 10. https://doi.org/10.1186/s12940-020-00690-y

Boies, A. M., Stettler, M. E. J., Swanson, J. J., Johnson, T. J., Olfert, J. S., Johnson, M., Eggersdorfer, M. L., Rindlisbacher, T., Wang, J., Thomson, K., Smallwood, G., Sevcenco, Y., Walters, D., Williams, P. I., Corbin, J., Mensah, A. A., Symonds, J., Dastanpour, R., & Rogak, S. N. (2015). Particle emission characteristics of a gas turbine with a double annular combustor. *Aerosol Science and Technology, 49*(9), 842–855. https://doi.org/10.1080/02786826.2015.1078452

Cambustion Ltd. (2016). *Aerodynamic aerosol classifier - user manual (V1.12)*.

Corbin, J. C., Schripp, T., Anderson, B. E., Smallwood, G. J., LeClercq, P., Crosbie, E. C., Achterberg, S., Whitefield, P. D., Miake-Lye, R. C., Yu, Z., Freedman, A., Trueblood, M., Satterfield, D., Liu, W., Oßwald, P., Robinson, C., Shook, M. A., Moore, R. H., & Lobo, P. (2022). Aircraft-engine particulate matter emissions from conventional and sustainable aviation fuel combustion: Comparison of measurement techniques for mass, number, and size. *Atmospheric Measurement Techniques, 15*(10), 3223–3242. https://doi.org/10.5194/amt-15-3223-2022

Crayford, A., Johnson, M., Sevcenco, Y., & Williams, P. (2014). *SAMPLE III SC.05 - studying, sAmpling and measuring of aircraft ParticuLate emission*. https://www.easa.europa.eu/document-library/research-reports/easa2010fc10-sc05.

Dastanpour, R., & Rogak, S. N. (2014). Observations of a correlation between primary particle and aggregate size for soot particles. *Aerosol Science and Technology, 48*(10), 1043–1049. https://doi.org/10.1080/02786826.2014.955565

Delhaye, D., Ouf, F.-X., Ferry, D., Ortega, I. K., Penanhoat, O., Peillon, S., Salm, F., Vancassel, X., Focsa, C., Irimiea, C., Harivel, N., Perez, B., Quinton, E., Yon, J., & Gaffie, D. (2017). The MERMOSE project: Characterization of particulate matter emissions of a commercial aircraft engine. *Journal of Aerosol Science, 105*, 48–63. https://doi.org/10.1016/j.jaerosci.2016.11.018

Durand, E. (2019). *Towards improved correction methodology for regulatory aircraft engine nvPM measurement (Thesis (PhD))*. Cardiff University.

Durand, E. F., Crayford, A. P., & Johnson, M. (2020). Experimental validation of thermophoretic and bend nanoparticle loss for a regulatory prescribed aircraft nvPM sampling system. *Aerosol Science and Technology*, 1–15. https://doi.org/10.1080/02786826.2020.1756212

Durand, E., Lobo, P., Crayford, A., Sevcenco, Y., & Christie, S. (2021). Impact of fuel hydrogen content on non-volatile particulate matter emitted from an aircraft auxiliary power unit measured with standardised reference systems. *Fuel, 287*, Article 119637. https://doi.org/10.1016/j.fuel.2020.119637

Durdina, L., Brem, B. T., Abegglen, M., Lobo, P., Rindlisbacher, T., Thomson, K. A., Smallwood, G. J., Hagen, D. E., Sierau, B., & Wang, J. (2014). Determination of PM mass emissions from an aircraft turbine engine using particle effective density. *Atmospheric Environment, 99*, 500–507. https://doi.org/10.1016/j.atmosenv.2014.10.018

Durdina, L., Brem, B. T., Elser, M., Schönenberger, D., Siegerist, F., & Anet, J. G. (2021). Reduction of nonvolatile particulate matter emissions of a commercial turbofan engine at the ground level from the use of a sustainable aviation fuel blend. *Environmental Science and Technology, 55*(21), 14576–14585. https://doi.org/10.1021/acs.est.1c04744

Durdina, L., Brem, B. T., Schönenberger, D., Siegerist, F., Anet, J. G., & Rindlisbacher, T. (2019). Non-volatile particulate matter emissions of a business jet measured at ground level and estimated for cruising altitudes. *Environmental Science and Technology*. https://doi.org/10.1021/acs.est.9b02513

EEDB. (2021). *ICAO engine emission Databank*. Hosted by the European Union Aviation Safety Agency (EASA).

Harper, J., Durand, E., Bowen, P., Pugh, D., Johnson, M., & Crayford, A. (2022). Influence of alternative fuel properties and combustor operating conditions on the nvPM and gaseous emissions produced by a small-scale RQL combustor. *Fuel, 315*, Article 123045. https://doi.org/10.1016/j.fuel.2021.123045

Hinds, W. C. (1998). *Aerosol technology: Properties behavior, and measurement of airborne particles*. Wiley-Interscience.

ICAO. (2017). *Annex 16 to the convention on international civil aviation: Environmental protection, volume II: Aircraft engine emissions* (4th ed.). International Civil Aviation Organisation.

ISO 15900:2009 (2014). ISO 15900:2009 - determination of particle size distribution - differential electrical mobility analysis for aerosol particles. Available at: https://www.iso.org/standard/39573.html. (Accessed 8 October 2018) Accessed.

Jonsdottir, H. R., Delaval, M., Leni, Z., Keller, A., Brem, B. T., Siegerist, F., Schönenberger, D., Durdina, L., Elser, M., Burtscher, H., Liati, A., & Geiser, M. (2019). Non-volatile particle emissions from aircraft turbine engines at ground-idle induce oxidative stress in bronchial cells. *Communications Biology, 2*(1), 90. https://doi.org/10.1038/s42003-019-0332-7

Kinsey, J. S., Giannelli, R., Howard, R., Hoffman, B., Frazee, R., Aldridge, M., Leggett, C., Stevens, K., Kittelson, D., Silvis, W., Stevens, J., Lobo, P., Achterberg, S., Swanson, J., Thomson, K., McArthur, T., Hagen, D., Trueblood, M., Wolff, L., … Durlicki, M. (2021). Assessment of a regulatory measurement system for the

determination of the non-volatile particulate matter emissions from commercial aircraft engines. *Journal of Aerosol Science, 154*, Article 105734. https://doi.org/10.1016/j.jaerosci.2020.105734

Kittelson, D., Khalek, I., McDonald, J., Stevens, J., & Giannelli, R. (2022). Particle emissions from mobile sources: Discussion of ultrafine particle emissions and definition. *Journal of Aerosol Science, 159*, Article 105881. https://doi.org/10.1016/j.jaerosci.2021.105881

Kittelson, D. B., Swanson, J., Aldridge, M., Giannelli, R. A., Kinsey, J. S., Stevens, J. A., Liscinsky, D. S., Hagen, D., Leggett, C., Stephens, K., Hoffman, B., Howard, R., Frazee, R. W., Silvis, W., McArthur, T., Lobo, P., Achterberg, S., Trueblood, M., Thomson, K., … Payne, G. (2022). Experimental verification of principal losses in a regulatory particulate matter emissions sampling system for aircraft turbine engines. *Aerosol Science and Technology, 56*(1), 63–74. https://doi.org/10.1080/02786826.2021.1971152

Lee, D. S., Fahey, D. W., Skowron, A., Allen, M. R., Burkhardt, U., Chen, Q., Doherty, S. J., Freeman, S., Forster, P. M., Fuglestvedt, J., Gettelman, A., De León, R. R., Lim, L. L., Lund, M. T., Millar, R. J., Owen, B., Penner, J. E., Pitari, G., Prather, M. J., Sausen, R., & Wilcox, L. J. (2021). The contribution of global aviation to anthropogenic climate forcing for 2000 to 2018. *Atmospheric Environment, 244*, Article 117834. https://doi.org/10.1016/j.atmosenv.2020.117834

Lobo, P., Durdina, L., Brem, B. T., Crayford, A. P., Johnson, M. P., Smallwood, G. J., Siegerist, F., Williams, P. I., Black, E. A., Llamedo, A., Thomson, K. A., Trueblood, M. B., Yu, Z., Hagen, D. E., Whitefield, P. D., Miake-Lye, R. C., & Rindlisbacher, T. (2020). Comparison of standardized sampling and measurement reference systems for aircraft engine non-volatile particulate matter emissions. *Journal of Aerosol Science, 105557*. https://doi.org/10.1016/j.jaerosci.2020.105557

Lobo, P., Durdina, L., Smallwood, G. J., Rindlisbacher, T., Siegerist, F., Black, E. A., Yu, Z., Mensah, A. A., Hagen, D. E., Miake-Lye, R. C., Thomson, K. A., Brem, B. T., Corbin, J. C., Abegglen, M., Sierau, B., Whitefield, P. D., & Wang, J. (2015). Measurement of aircraft engine non-volatile PM emissions: Results of the aviation-particle regulatory instrumentation demonstration experiment (A-PRIDE) 4 campaign. *Aerosol Science and Technology, 49*(7), 472–484. https://doi.org/10.1080/02786826.2015.1047012

Olfert, J., & Rogak, S. (2019). Universal relations between soot effective density and primary particle size for common combustion sources. *Aerosol Science and Technology, 53*(5), 485–492. https://doi.org/10.1080/02786826.2019.1577949

RAPTOR Project Library. (2022). RAPTOR. Available at: https://aviation-pm.eu/project-library/. (Accessed 7 October 2022) Accessed.

SAE International. (2019). ARP 6481- procedure for the calculation of sampling line penetration functions and line loss correction factors. https://doi.org/10.4271/ARP6481.

SAE International. (2020). *AIR 6241-procedure for the continuous sampling and measurement of non-volatile particle emissions from aircraft turbine engines*.

SAE International. (2021). *ARP 6320A - procedure for the continuous sampling and measurement of non-volatile particulate matter emissions from aircraft turbine engines*. https://doi.org/10.4271/ARP6320

SAE International. (2022). AIR 6504 - procedure for the calculation of sampling system penetration functions and system loss correction factors. https://doi.org/10.4271/AIR6504.

Saffaripour, M., Thomson, K. A., Smallwood, G. J., & Lobo, P. (2019). A review on the morphological properties of non-volatile particulate matter emissions from aircraft turbine engines. *Journal of Aerosol Science, 105467*. https://doi.org/10.1016/j.jaerosci.2019.105467

Seinfeld, J. H., & Pandis, S. N. (2016). *Atmospheric chemistry and physics: From air pollution to climate change*. John Wiley & Sons.

Xue, J., Li, Y., Wang, X., Durbin, T. D., Johnson, K. C., Karavalakis, G., Asa-Awuku, A., Villela, M., Quiros, D., Hu, S., Huai, T., Ayala, A., & Jung, H. S. (2015). Comparison of vehicle exhaust particle size distributions measured by SMPS and EEPS during steady-state conditions. *Aerosol Science and Technology, 49*(10), 984–996. https://doi.org/10.1080/02786826.2015.1088146

Zimmerman, N., Godri Pollitt, K. J., Jeong, C.-H., Wang, J. M., Jung, T., Cooper, J. M., Wallace, J. S., & Evans, G. J. (2014). Comparison of three nanoparticle sizing instruments: The influence of particle morphology. *Atmospheric Environment, 86*, 140–147. https://doi.org/10.1016/j.atmosenv.2013.12.023